

# Elementary Calcium-Release Units Induced by Inositol Trisphosphate

John H. Horne and Tobias Meyer\*

The extent to which inositol 1,4,5-trisphosphate (InsP<sub>3</sub>)-induced calcium signals are localized is a critical parameter for understanding the mechanism of effector activation. The spatial characteristics of InsP<sub>3</sub>-mediated calcium signals were determined by targeting a dextran-based calcium indicator to intracellular membranes through the in situ addition of a geranylgeranyl lipid group. Elementary calcium-release events observed with this indicator typically lasted less than 33 milliseconds, had diameters less than 2 micrometers, and were uncoupled from each other by the calcium buffer EGTA. Cellwide calcium transients are likely to result from synchronized triggering of such local release events, suggesting that calcium-dependent effector proteins could be selectively activated by localization near sites of local calcium release.

Inositol 1,4,5-trisphosphate-induced increases in cytosolic Ca<sup>2+</sup> concentration are essential for a large number of receptor-initiated signaling pathways in nearly all cell types (1). Although InsP<sub>3</sub>-mediated Ca<sup>2+</sup> transients are often largely uniform across the cytosol, it has been proposed that they result from the synchronized triggering of highly localized Ca<sup>2+</sup>-release events (2), much like those of ryanodine receptor channels (3). Such localized events could target specific Ca<sup>2+</sup>-sensitive proteins, thus increasing the precision by which InsP<sub>3</sub>-mediated signal transduction activates downstream targets.

Resolving the spatial aspects of Ca<sup>2+</sup> signaling is problematic when the Ca<sup>2+</sup> indicator itself is readily diffusible, and could be more accurately resolved with an immobilized Ca<sup>2+</sup> indicator. To design such an indicator, we relied on the endogenous posttranslational protein-modification machinery to add a geranylgeranyl lipid group to a peptide containing a COOH-terminal CAAX sequence. This CAAX peptide was coupled to dextran-calcium green with a homobifunctional amine cross-linker (4). The resulting indicator (CAAX green) was soluble and uniformly distributed in the cytosol immediately after electroporation into rat basophilic leukemia (RBL) cells (5) and was then processed by addition of a geranylgeranyl lipid group within 3 hours (Fig. 1) (6). This processing led to the nonspecific localization of CAAX green to internal membranes, as indicated by its localization to the plasma membrane, nuclear membrane, and various reticular structures in the cytosol (Fig. 1).

The time course of membrane attachment of CAAX green was more accurately determined by two additional approaches:

(i) The diffusion coefficient, as determined by photobleaching experiments (7), was  $6.55 \pm 1.1 \mu\text{m}^2/\text{s}$  ( $n = 9$ ) immediately after electroporation and decreased to  $0.64 \pm 0.11 \mu\text{m}^2/\text{s}$  ( $n = 4$ ) at 1 hour. (ii) Maximal retention of CAAX green fluorescence in digitonin-permeabilized cells was reached within 45 min ( $95 \pm 12\%$ ,  $n = 5$ ) (8). These results suggest that CAAX green is lipid-modified in less than 1 hour after introduction into the cytosol, resulting in membrane attachment and immobilization.

A rapid increase in cytosolic Ca<sup>2+</sup> concentration (<66 ms) (Fig. 2A) was triggered when a saturating amount of InsP<sub>3</sub> was uniformly released throughout the cell by ultraviolet (UV)-mediated photorelease of caged InsP<sub>3</sub> (9). Subtracted images were used to determine the spatial aspects of this rapid increase (Fig. 2B) (10). In response to

a maximal dose, InsP<sub>3</sub>-mediated Ca<sup>2+</sup> release was largely uniform across the cell, similar to the spatial characteristics observed for receptor-mediated Ca<sup>2+</sup> transients observed in these and other cells (1, 11). Similar results were observed in 10 cells analyzed.

Local Ca<sup>2+</sup>-release events have been observed in *Xenopus leavis* oocytes and pancreatic acinar cells in response to minimal increases in InsP<sub>3</sub> concentration (12). These events have thus far been observed only in specialized regions of cells and may result from nonuniform distributions of InsP<sub>3</sub> receptors or a locally increased sensitivity to InsP<sub>3</sub> (13). Nevertheless, it has been proposed that receptor-mediated Ca<sup>2+</sup> transients in all cell types are the result of rapid coupling of individual, all-or-none Ca<sup>2+</sup>-release units (2). The coupling between such local release units would be mediated by Ca<sup>2+</sup> diffusion and triggered by Ca<sup>2+</sup> activation of InsP<sub>3</sub>-dependent Ca<sup>2+</sup> release (14). We reasoned that if such elementary Ca<sup>2+</sup>-release units were the building blocks of cellwide Ca<sup>2+</sup> transients, individual units could be resolved by blocking the Ca<sup>2+</sup>-mediated synchronization with the slow Ca<sup>2+</sup> buffer EGTA.

In the presence of 0.5 to 1 mM intracellular EGTA, the rise time of the global Ca<sup>2+</sup> increase induced by a saturating dose of InsP<sub>3</sub> was 15 times longer than in the absence of EGTA (Fig. 2C). This suggests that Ca<sup>2+</sup> diffusion is required to generate the rapid, global release event observed in Fig. 2, A and B. Strikingly, underlying this slowed release were rapid, localized, and stochastic release events that often changed

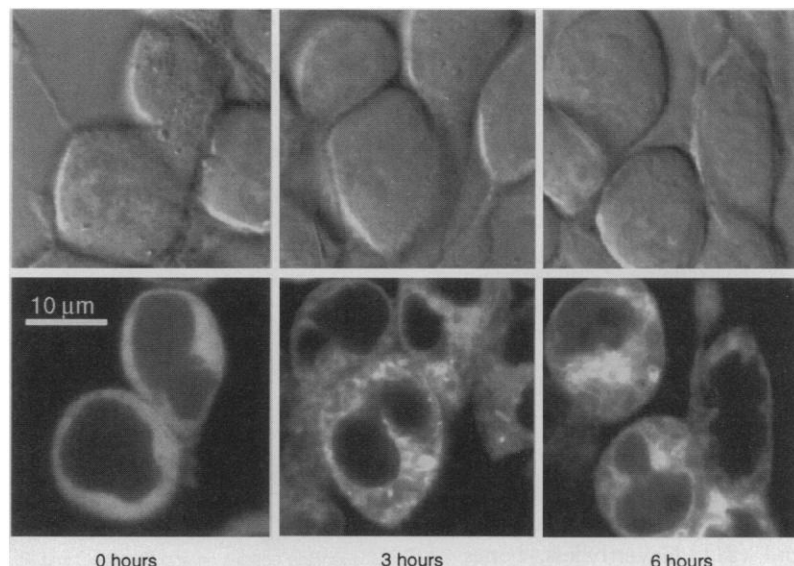


**Fig. 1.** Localization of CAAX green to internal membranes in RBL cells. Differential interference contrast (DIC) and confocal fluorescence images with fluorescein optics are shown for cells at 0, 3, and 6 hours after electroporation (7). Bar, 10  $\mu\text{m}$  for all images. The dissociation constant ( $K_d$ ) of membrane-bound CAAX green is 650 nM (4).

Department of Cell Biology, Duke University Medical Center, Durham, NC 27710, USA.

\*To whom correspondence should be addressed.

location in subsequent frames (Fig. 2D). Similar results were observed in six cells analyzed. Under these conditions the basal  $\text{Ca}^{2+}$  concentration was the same with EGTA [ $51 \pm 12 \text{ nM}$  ( $n = 10$ )] and without EGTA [ $51 \pm 17 \text{ nM}$  ( $n = 10$ )]. These images reveal the existence of elementary  $\text{Ca}^{2+}$ -release units and suggest that these units were resolved only because EGTA reduced the probability of triggering individual release events. Lower EGTA concentrations (100 to 250  $\mu\text{M}$ ) were not sufficient to uncouple these elementary  $\text{Ca}^{2+}$ -release units. One can therefore calculate that the time required for coupling of release events is  $\sim 1 \text{ ms}$  (15).

It is difficult to determine the exact di-

mensions of individual release events at the resolution of light microscopy. We determined an upper limit to the size of localized  $\text{Ca}^{2+}$ -release events by marking locations with a 6% or higher increase in intensity (Fig. 3A). The size distribution of these areas was represented as a histogram, with the number of events plotted as a function of the maximal diameter of the area (Fig. 3B).  $\text{Ca}^{2+}$ -release events with diameters from 0 to 2  $\mu\text{m}$  were most frequently observed. A plot of the local frequency of  $\text{Ca}^{2+}$ -release events showed that they are triggered in all regions of the cytosol, with slightly higher frequencies in the perinuclear and plasma membrane regions (16). Comparison of the distribution of release events with the distribu-

tion of indicator showed no correlation, indicating that the localization of release events was not an artifact resulting from uneven indicator distribution.

We analyzed the time course of  $\text{Ca}^{2+}$ -release events by comparing the  $\text{Ca}^{2+}$ -release kinetics measured from the whole cell to that measured at several  $1\text{-}\mu\text{m}^2$  boxes in various regions of the cell (Fig. 3C). This comparison showed that different regions of the cell experience different release kinetics. The local transient can coincide with, lag behind, or precede the global increase, and rapid local increases were often observed. The duration of these shorter events was typically less than 100 ms, with many events below the resolution limit of

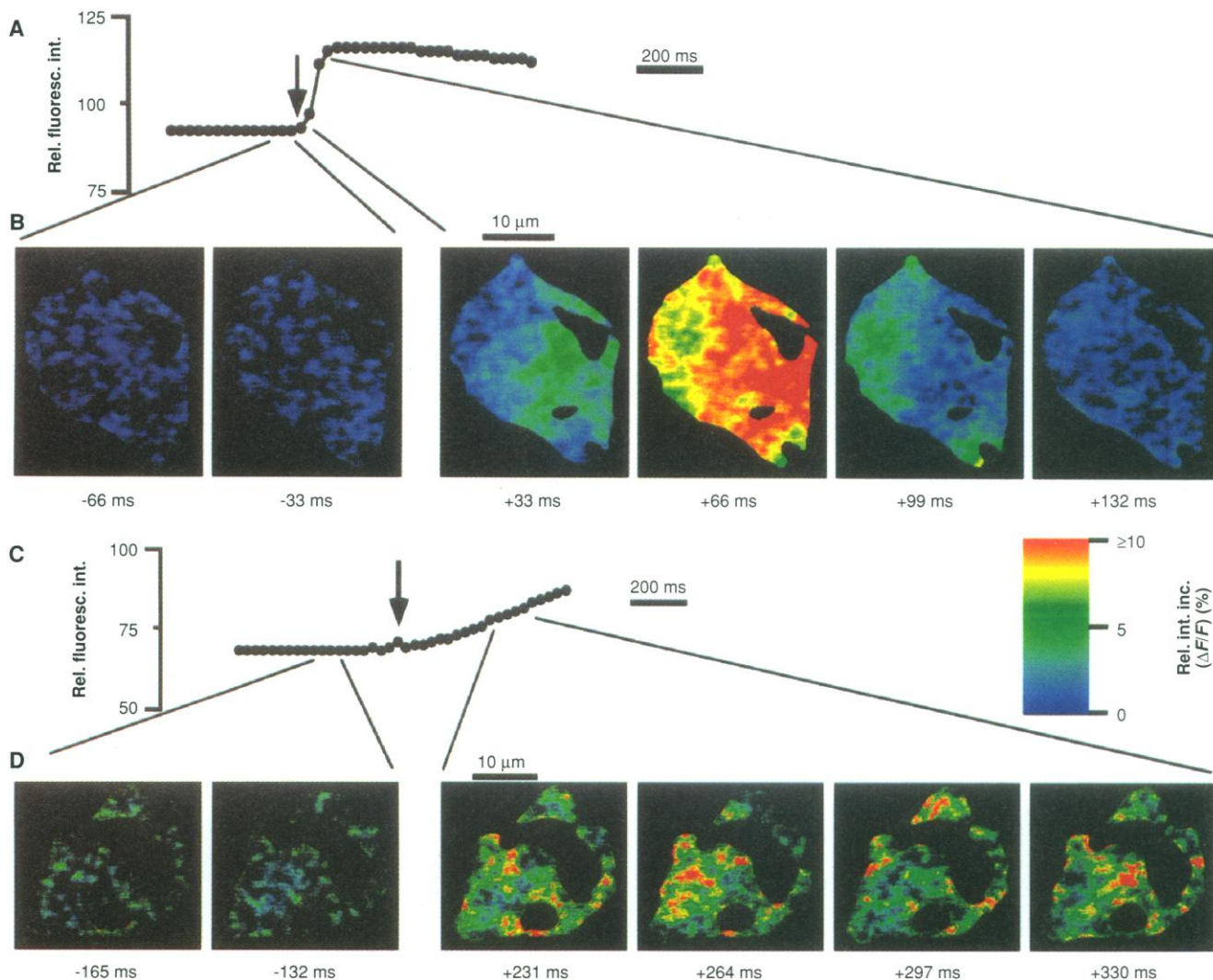


**Fig. 2.** Increase in  $\text{Ca}^{2+}$  concentration after UV laser-triggered photorelease of saturating amounts of  $\text{InsP}_3$  in the absence and presence of EGTA. **(A)** The change in average relative fluorescence intensity of CAAX green in an individual cell as a function of time. Images were recorded every 33 ms and corrected for background fluorescence before the average fluorescence intensity was determined. The arrow indicates a 20-ms UV-laser pulse illuminating the entire cell. The peak free  $\text{Ca}^{2+}$  concentration was estimated to be 400 nM with the in situ  $K_d$  calibration of the indicator (4). **(B)** Subtracted images show a near uniform increase in local  $\text{Ca}^{2+}$  con-

centration. A 10% increase in CAAX green fluorescence corresponds to a  $\sim 50 \text{ nM}$  increase in the free  $\text{Ca}^{2+}$  concentration (4). Consecutive images were recorded at the times indicated (relative to the UV pulse). Decreases in  $\text{Ca}^{2+}$  concentration are shown in black. **(C)** Same intensity trace as in (A) but measured in the presence of EGTA. An estimated intracellular concentration of 0.5 to 1 mM EGTA was introduced by addition of 20 mM extracellular EGTA during the electroporation of caged  $\text{InsP}_3$ . **(D)** Subtracted images in the presence of EGTA show localized  $\text{Ca}^{2+}$ -release events.

33 ms. Therefore, although the global increase in  $\text{Ca}^{2+}$  elicited by  $\text{InsP}_3$  is slowed in the presence of EGTA, the localized  $\text{Ca}^{2+}$ -release events remained rapid. The effect of EGTA appears to be to prevent synchronization by lowering the probability of triggering local  $\text{Ca}^{2+}$ -release events.

The noise contribution to the observed local increases in fluorescence intensity was determined by histogram analysis of the amplitude of fluorescence intensity fluctuations (Fig. 3D). No significant difference was observed between the fluctuations at basal  $\text{Ca}^{2+}$  concentration (top panel) and those of cells with thapsigargin-depleted  $\text{Ca}^{2+}$  stores (middle panel), suggesting that the small basal fluctuations are not spontaneous release events. In contrast, the average local intensity fluctuations increased by 260% after an increase in  $\text{InsP}_3$  concentration, demonstrating that the observed  $\text{Ca}^{2+}$ -release events are significantly above the photon noise (bottom panel).

An estimate of the  $\text{Ca}^{2+}$  current responsible for individual release events can be

made from the local change in fluorescence intensity. At least 30 pA of current is required to generate a 10% increase in CAAX green fluorescence, assuming that a release volume of  $1 \mu\text{m}^3$  contains more than  $50 \mu\text{M}$  of  $\text{Ca}^{2+}$  buffer. This is similar to the current responsible for  $\text{Ca}^{2+}$  "puffs" in *Xenopus* oocytes (10 to 20 pA) (12). The conductance of  $\text{InsP}_3$ -receptor channels incorporated into lipid bilayers is  $\sim 2 \text{ pA}$  (14), suggesting that the observed localized events are likely to result from the simultaneous opening of several  $\text{InsP}_3$ -gated  $\text{Ca}^{2+}$  channels.

Our study shows that  $\text{InsP}_3$ -induced  $\text{Ca}^{2+}$  transients are likely the result of synchronized triggering of elementary  $\text{Ca}^{2+}$ -release units. Because the amplitudes of localized release events were similar at increasing  $\text{Ca}^{2+}$  concentrations, it is likely that  $\text{Ca}^{2+}$  does not control the size of  $\text{Ca}^{2+}$ -release events but instead regulates the stochastic probability at which elementary  $\text{Ca}^{2+}$ -release units are triggered. The existence of localized all-or-none  $\text{Ca}^{2+}$ -release

events suggests that  $\text{Ca}^{2+}$ -dependent enzymes can be selectively activated by their localization with, or translocation to, such local sites of  $\text{Ca}^{2+}$  release.

## REFERENCES AND NOTES

1. M. J. Berridge, *Nature* **361** 315 (1993).
2. M. D. Bootman and M. J. Berridge, *Cell* **83**, 675 (1995).
3. M. B. Cannell and H. Cheng, W. J. Lederer, *Science* **268**, 1045 (1995); M. T. Nelson *et al.*, *ibid.* **270**, 633 (1995); M. G. Klein *et al.*, *Nature* **379**, 455 (1996).
4. The  $\text{NH}_2$ -terminal free amine of a CAAX peptide,  $\text{NH}_2\text{-Thr-Arg-Gln-Gln-Arg-Arg-Ala-Cys-Ser-Leu-Leu-COO}^-$  (Howard Hughes facility, Stanford University), was covalently linked to dextran-calcium green with available free amino groups (provided by M. Kuhn, Molecular Probes, Eugene, OR) with a homobifunctional amine-reactive cross-linker, BS<sup>3</sup> [*bis*-(sulfosuccinimidyl) suberate] (Pierce, Rockford, IL). Details of the synthesis are reported by J. H. Horne and T. Meyer (in preparation).
5. RBL cells were grown as described [E. Oancea and T. Meyer, *J. Biol. Chem.* **271**, 17253 (1996)]. Cells were loaded with CAAX green by means of a small-volume electroporation device (M. Teruel and T. Meyer, in preparation) 6 to 8 hours before experiments. The final concentration of CAAX green in electroporated cells was estimated to be  $50 \mu\text{M}$ . Differential interference contrast and confocal fluorescence images were recorded on a Zeiss confocal microscope.
6. F. L. Zhang and P. J. Casey, *Annu. Rev. Biochem.* **65**, 241 (1996).
7. H. Yokoe and T. Meyer, *Nature Biotechnol.* **14**, 1252 (1996).
8. The time course of CAAX green processing was determined in digitonin-permeabilized cells ( $15 \mu\text{g/ml}$ ). Total cell fluorescence was determined from background-subtracted images with Image-1 software. For comparison between experiments, the data were expressed as a percentage of the maximal fluorescence retained, which varied between 60 and 80% of the fluorescence before digitonin permeabilization. The incomplete retention during permeabilization is most likely due to a partial digitonin destruction of cells.
9. Caged  $\text{InsP}_3$  [J. W. Walker *et al.*, *Biochemistry* **28**, 3272 (1989)] was introduced into cells by electroporation 10 min before each experiment (estimated cytosolic concentration  $\sim 100 \mu\text{M}$ ). Cells were maintained at  $37^\circ\text{C}$  throughout the experiment. The apparent basal free  $\text{Ca}^{2+}$  concentration was calibrated as described [R. Y. Tsien, *ibid.* **19**, 2396 (1980)].
10. CAAX green fluorescence was monitored with a Nikon confocal microscope (Middleton, WI), and images were recorded every 33 ms with a Bitflow 64-Mb RAM (random-access memory) imaging board and Eye Image software (IO Industries, London, Ontario, Canada). Image-1 or Eye Image software was used for all image analysis. The confocal setting used resulted in a Z-section resolution of  $\sim 2 \mu\text{m}$ . Fluorescent images were processed in several steps: low-pass filter (8 pixels, corresponding to  $\sim 0.9 \mu\text{m}$ ), background subtraction, masking for the cytosolic region, determining the ratio to an averaged image collected before the UV pulse (50 frames) to correct for the uneven indicator distribution, and subtraction of subsequent images by an algorithm that shows only  $\text{Ca}^{2+}$  increases but not decreases during the time interval.
11. T. Meyer and L. Stryer, *Annu. Rev. Biophys. Biochem.* **20**, 153 (1991).
12. Y. Yao, J. Choi, I. Parker, *J. Physiol.* **482**, 533 (1995); P. Thorn, A. M. Lawrie, P. M. Smith, V. D. Gallacher, O. H. Petersen, *Cell* **74**, 661 (1993).
13. K. Hirose and M. Iino, *Nature* **372**, 791 (1994).
14. M. Iino and M. Endo, *ibid.* **360**, 76 (1992); E. A. Finch,

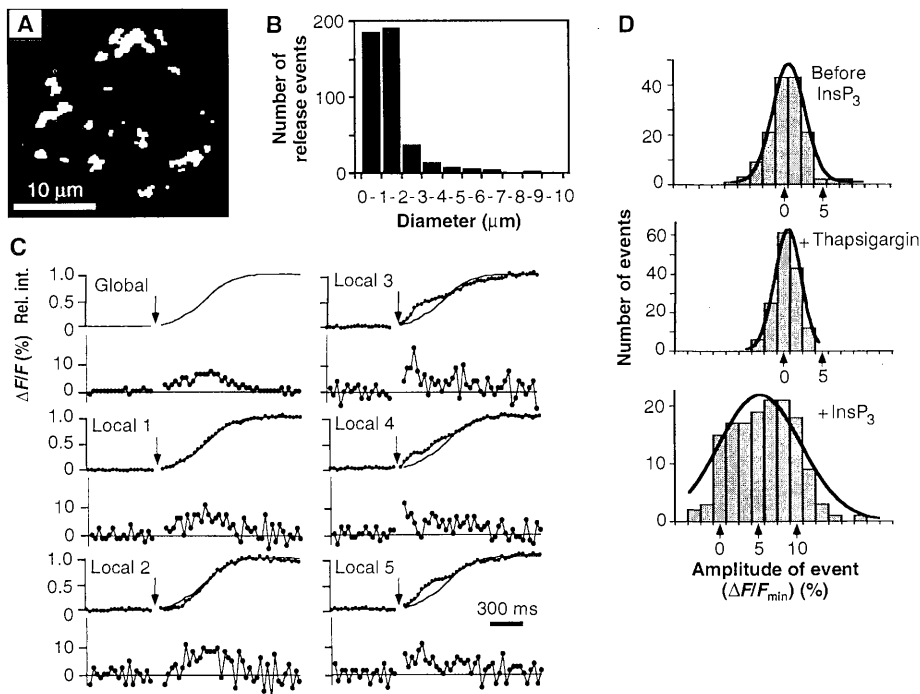


**Fig. 3.** Analysis of elementary  $\text{Ca}^{2+}$ -release units. Subtracted images the same as those shown in Fig. 2D were used to analyze the spatial distribution of local  $\text{Ca}^{2+}$ -release events. (A) A threshold of 6%  $\Delta F/F$  was imposed on the subtracted image, and the resulting binary image shows areas of the cell above this threshold in white and areas below in black. (B) Histogram of the number of release events as a function of the size of elementary release units (largest diameter). A series of 20 consecutive images during the rising phase (Fig. 3) were processed as in (A) and analyzed with Image-1 object analysis. (C) The time course of fluorescence increases from several regions of the cell analyzed in two ways. (Top) Relative local fluorescence increase; (bottom) subtractive plot showing the increase in fluorescence relative to the previous frame. The global increase across the cell is shown in the top left panel and is also plotted in each of the local release traces (solid line). (D) Comparison of the fluctuations in local fluorescence intensity in unstimulated cells (top), after addition of thapsigargin (middle), and after uncaging of  $\text{InsP}_3$  (bottom). Local fluctuations were plotted by counting the number of times a given change in local fluorescence intensity was measured (in every 33 ms, at different  $1\text{-}\mu\text{m}^2$  areas). Gaussian fits to each histogram are shown as solid lines.

- T. J. Turner, S. M. Goldin, *Science* **252**, 443 (1991); I. Bezprozvanny, J. Watras, B. E. Ehrlich, *Nature* **351**, 751 (1991); J. H. Horne and T. Meyer, *Biochemistry* **34**, 12738 (1995).
15. M. D. Stern, *Cell Calcium* **13**, 183 (1992).
16. J. H. Horne and T. Meyer, data not shown.
17. We thank C. Nicchitta, G. Augustine, P. Casey, J. Thissen, and K. Dolinski for helpful discussions, and

M. Teruel for setting up the electroporation apparatus and the rapid image capturing system. Synthesis of caged  $\text{InsP}_3$  was performed in the laboratory of J. Walker (University of Wisconsin, Madison, WI; supported by NIH grant P01-HL-47053). Supported by NIH grants RO1-GM-48113 and GM-51457.

22 October 1996; accepted 28 April 1997

## Shared Motor Error for Multiple Eye Movements

R. J. Krauzlis,\* M. A. Basso, R. H. Wurtz

Most natural actions are accomplished with a seamless combination of individual movements. Such coordination poses a problem: How does the motor system orchestrate multiple movements to produce a single goal-directed action? The results from current experiments suggest one possible solution. Oculomotor neurons in the superior colliculus of a primate responded to mismatches between eye and target positions, even when the animal made two different types of eye movements. This neuronal activity therefore does not appear to convey a command for a specific type of eye movement but instead encodes an error signal that could be used by multiple movements. The use of shared inputs is one possible strategy for ensuring that different movements share a common goal.

Distinct sensory and motor functions are localized in different regions of the brain. In the visual system, for example, attributes such as form and motion may be processed in largely separate areas (1). However, it is not known how the results of such specialized processing are combined to produce a single coherent percept, an issue that is often referred to as the "binding problem" (2). A similar question applies to motor systems, because most actions, despite their unitary appearance, are composed of multiple movements, each controlled by different brain regions. For example, when we visually search the contents of a room, we use a combination of saccadic and pursuit eye movements, interspersed with periods of fixation. The individual movements are quite distinct: Saccades are brief high-velocity movements that interrupt fixation and abruptly reorient the eyes toward eccentric visual targets, whereas pursuit is a continuous slow movement that smoothly rotates the eyes to maintain alignment with moving targets. These movements are also mediated by largely distinct neuroanatomical pathways (3). The anatomical pathways underlying saccades and fixation include such cortical regions as the lateral intraparietal sulcus and the frontal eye fields and such subcortical regions as the superior colliculus and brainstem reticular formation. In contrast, the pathways underlying pursuit

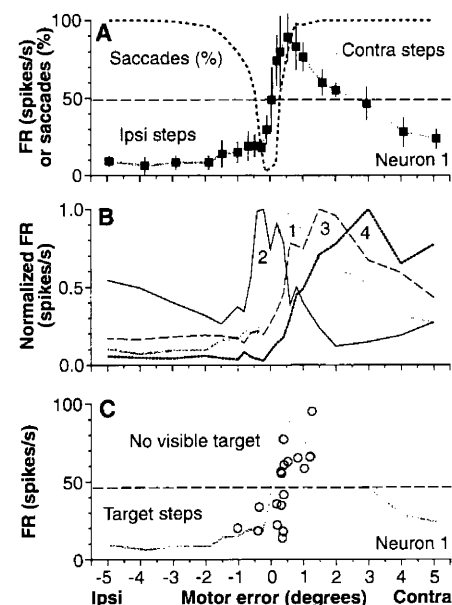
include such cortical regions as the middle temporal area and medial superior temporal sulcus and such subcortical regions as the basilar pons and cerebellum. What enables these different oculomotor subsystems to interact harmoniously, despite this modular design? One possibility is that they overlap at early stages of movement preparation. For example, the visual capture of a single target with different types of eye movements would be facilitated if they shared a mechanism for target selection. Indeed, re-

cent behavioral experiments have suggested that there are common inputs for triggering the onset of saccades and pursuit (4). The data from our present study provide evidence for overlap in the underlying neural pathways.

Our experiments focused on the superior colliculus (SC) of primates, a laminated mid-brain structure known to be important for the generation of saccadic eye movements (5). The superficial layers of the SC contain visually responsive neurons that form a retinotopic map of visual space, whereas the deeper layers contain saccade-related neurons that form a corresponding motor map. In most of this motor map, neurons in the intermediate and deep layers increase their firing rate before, or burst during, saccades of a particular direction and amplitude. However, in the portion of the map corresponding to the fovea, located at the rostral end of the SC, neurons are tonically active during periods of steady fixation and decrease their firing rate for most saccades. Accordingly, these neurons have been referred to as "fixation cells" in the cat (6) and monkey (7) and are believed to be important for determining when saccades are initiated. We now show that these neurons report mismatches between eye and target positions as do neurons elsewhere in the SC motor map. Furthermore, they are also modulated by the small mismatches that occur during pursuit eye movements. Together, these two results suggest that SC neurons might encode a more general form of motor error rather than commands for specific movements.

We first show that neurons in the rostral

**Fig. 1.** Tuning of neurons in the rostral SC for small mismatches between eye and target positions. **(A)** Modulation in the firing rate (FR) of neuron 1 recorded after small ipsiversive (ipsi) and contraversive (contra) steps of a target presented on a homogeneous background. Square symbols plot the average firing rate from 12 trials over an interval beginning 100 ms after the step and lasting either 100 ms or until 8 ms before any corrective saccade. Error bars indicate  $\pm 1$  SD. Dotted line indicates the percentage of trials in which each amplitude of the target step elicited a saccade. Saccades were detected as any eye movement exceeding  $5^\circ/\text{s}$  and  $800^\circ/\text{s}^2$ ; these criteria identified saccades as small as  $0.05^\circ$ . Dashed line indicates the average firing rate with no target steps. **(B)** Modulation of four rostral SC neurons (numbers 1 through 4) after small steps; all were recorded from the right SC of one monkey. The data have been normalized so that the peak of each curve equals 1. **(C)** Firing rate of neuron 1 recorded as the monkey maintained fixation after the visual stimulus was extinguished. Circles indicate the average firing rate during each of 18 saccade-free intervals lasting 73 to 230 ms and are plotted as a function of the average motor error during each interval. Dashed line indicates the average firing rate across all intervals. The superimposed gray curve shows the discharge of the same neuron when the stimulus was still present, as in (A).



Laboratory of Sensorimotor Research, National Eye Institute, National Institutes of Health, Bethesda, MD 20892, USA.

\*To whom correspondence should be addressed at Salk Institute, Post Office Box 85800, San Diego, CA 92186, USA.